

# Experimental Studies of Position Control of Linkage based Robotic Finger

N. Z. Azlan and H. Yamaura

**Abstract**—The experimental study of position control of a light weight and small size robotic finger during non-contact motion is presented in this paper. The finger possesses fingertip pinching and self adaptive grasping capabilities, and is made of a seven bar linkage mechanism with a slider in the middle phalanx. The control system is tested under the Proportional Integral Derivative (PID) control algorithm and Recursive Least Square (RLS) based Feedback Error Learning (FEL) control scheme to overcome the uncertainties present in the plant. The experiments conducted in Matlab Simulink and xPC Target environments show that the overall control strategy is efficient in controlling the finger movement.

**Keywords**—Anthropomorphic finger, position control, feedback error learning, experimental study

## I. INTRODUCTION

COMPACT anthropomorphic hands are specifically developed to serve the function of a human hand whilst having the same natural physical appearance and weight as close as possible. This type of hand plays a vital role in the prosthetics application. The amputees who lost their arms due to accidents wear prosthetic hands and use these instruments to facilitate them in performing their daily activities. Besides that, this type of hand is also significant in the humanoid field, where the robots are required to carry out tasks in the same working environment as human beings and are expected to achieve high performance and capability as human.

The main challenge in the design problem is to develop a mechanism and control algorithm that can realize the same shape, size and weight but operates and moves similar to a human hand since there are not many efficient components that are small and light enough to realize practical hand movements [1]. Some examples of previous hands with high functionality but bulky and heavy due to the number of sensors incorporated include [2] and [3]. The fingers in [4] and [5] are light in weight and small in size, which are close to a human hand physical appearance, but they are limited to grasping functions only.

This paper presents the experimental study of the position control a compact finger with self adaptive capability and fingertip pinching. The finger is composed of seven bar linkages and a lead screw mechanism to adjust the middle phalanx's effective link in performing grasping and fingertip pinching task. The simulation study of the finger under

Proportional Integral Derivative (PID) control has been presented in [6]. This study investigates the effectiveness of PID controller and Recursive Least Square (RLS) based Feedback Error Learning (FEL) control strategy in real time implementation through experimental works. FEL control scheme is applied to overcome the uncertainties present in the robotic finger. RLS algorithm is chosen to learn the inverse plant model in the FEL feedforward loop since it is easy to implement, computationally efficient and does not need any tedious effort in initializing the learning parameters.

This paper is organized as follows; the finger mechanism and mathematical model are described briefly in Section II and Section III respectively. The RLS based FEL control algorithm is presented in Section IV, Section V provides the explanation of the experimental hardware set up, results are discussed in Section VI and finally conclusions are drawn in Section VII.

## II. ROBOTIC FINGER MECHANISM

The robotic finger is built from seven bar mechanism with a slider in the middle phalanx as illustrated in Fig. 1. Link 1 is fixed and other linkages are able to rotate. The main force exerted by the finger is provided by Motor A at link 2. The motor also is responsible for the rotation of the whole finger. Motor B is a low torque micro-motor which actuates the slider mechanism to turn the distal phalanx during pinching operation. The robotic finger possesses a lighter weight and closer size to human's finger whilst able to provide the sufficient force required to accomplish both grasping and pinching tasks. There is no gear transmission within the phalanges and the number of force sensors can be reduced since it has self adaptive grasping capability.

During grasping operation, the distal phalanx's pin remains at point C or is moved to point C by the Motor B to lengthen the effective distance between the pin and point A. Therefore the final grasping configuration can be realized as in Fig. 2. During this operation, the finger behaves as a linkage based underactuated finger mechanism with self adaptable capability. In pinching function, motor B moves distal phalanx's pin along the guiding slot from the rest position at point C to point B on the upper link of the middle phalanx. This shortens the effective length between the pin and point A until the finger reaches the final pinching configuration as illustrated in Fig. 3. Motor A provides the input torque to turn the whole finger to pinch thin and small objects.

N. Z. Azlan and H. Yamaura are with the Department of Mechanical and Control Engineering, Graduate School of Science and Engineering, Tokyo Institute of Technology, Ookayama 2-12-1-I3-10, Meguro-ku, Tokyo, 158-8552, Japan. (e-mail: zainulazlan.n.aa@m.titech.ac.jp, yamaura@mech.titech.ac.jp).

## III. MATHEMATICAL MODEL

Fig. 4 represents the seven bar linkages compact robotic finger. The finger notations are summarized as in Table 1. The dynamic model for the finger is derived based on the 4 bar planar linkage [7-8] and hybrid actuator [9] models.

To reduce the modeling effort, it is assumed that the finger operate in horizontal plane, therefore the potential energy due to the gravitational effect is negligible. It is also assumed that the model is made for the finger while non-contact mode, in which the distal and middle phalanx is not in contact with any object. In this case, the angle between link 4 and link 5 are constant or in other words, the two links are assumed to be coupled in this work.

From Lagrange's equation, the mathematical model of a robotic system can be represented as

$$\frac{d}{dt} \left( \frac{\partial K}{\partial \dot{\theta}_j} \right) - \frac{\partial K}{\partial \theta_j} + \frac{\partial P_o}{\partial \theta_j} = T_j, \quad (1)$$

where  $K$  is the kinetic energy,  $P_o$  is the potential energy of the system,  $T$  is the generalized torque and the subscript  $j$  denotes the generalized coordinates.

Choosing the generalized coordinates as the input angle to link 2,  $\theta_2$  and the input angle to the slider mechanism,  $\theta_s$ , the torque due to the linkages can be expressed using (1) in terms of  $\theta_2$  and  $\theta_s$  as [6]

$$A\ddot{\theta}_2(t) + \frac{1}{2} \frac{dA}{d\theta_2} \dot{\theta}_2^2(t) = T_2 \quad (2)$$

$$\left( B + m_r \left( -\frac{P}{2\pi} \right)^2 + J_r \right) \ddot{\theta}_s(t) + \frac{1}{2} \frac{dB}{d\theta_s} \dot{\theta}_s^2(t) = T_s \quad (3)$$

Integrating the torques in (2) and (3) with the dynamic equation of an electrical motor, the dynamic behaviour of the finger during pinching operation can be finally described by second order differential equations as

$$\ddot{\theta}_2(t) = A_0 (A_1 \dot{\theta}_2^2(t) + A_2 \dot{\theta}_2(t) + A_3 i_2(t) + A_4) \quad (4)$$

$$\ddot{\theta}_s(t) = B_0 (B_1 \dot{\theta}_s^2(t) + B_2 \dot{\theta}_s(t) + B_3 i_s(t) + B_4) \quad (5)$$

where

$$\begin{aligned} A_0 &= \frac{1}{A + J_{m2} N_2^2}, & A_1 &= -\frac{1}{2} \frac{dA}{d\theta_2}, \\ A_2 &= -N_2^2 B_{v2}, & A_3 &= N_2 K_{t2}, & A_4 &= -T_{f2}, \\ B_0 &= \frac{1}{B + m_r \left( -\frac{P}{2\pi} \right)^2 + J_r + J_{ms} N_s^2}, & B_1 &= -\frac{1}{2} \frac{dB}{d\theta_s}, \\ B_2 &= -N_s^2 B_{v2s}, & B_3 &= N_s K_{ts}, & B_4 &= -T_{fs} \end{aligned} \quad (6)$$

where  $J_{mj}$  is the moment of inertia of  $j$ th motor,  $B_{vj}$  is the viscous damping coefficient of the  $j$ th motor,  $K_{tj}$  is the torque constant of

 TABLE I  
LINKAGE PARAMETERS NOTATION

Notation	Parameter
$\theta_i$	angular displacement of $i$ th link
$\dot{\theta}_i$	angular velocity of $i$ th link
$\ddot{\theta}_i$	angular acceleration of $i$ th link
$m_i$	mass of $i$ th link
$m_r$	mass of slider
$l_i$	length of $i$ th link
$J_i$	moment of inertia of $i$ th link
$J_r$	moment of inertia of slider
$l_i$	length of $i$ th link
$r_i$	mass centre of $i$ th link
$\delta_i$	angle between the $i$ th link's edge and its centroid
$X_{oi}, Y_{oi}$	$x$ and $y$ coordinate of $i$ th link's origin
$X_{ci}, Y_{ci}$	$x$ and $y$ coordinate of $i$ th link's centroid from its origin

the  $j$ th motor,  $i_j$  is the armature current of the  $j$ th motor,  $N_j$  is the gear ratio of the  $j$ th motor.  $T_{fj}$  is the dry friction of the  $j$ th motor, which is assumed to be constants for modeling simplicity,  $L_j$  is the armature inductance of  $j$ th motor,  $R_j$  is the resistance of  $j$ th motor,  $K_{vj}$  is the voltage constant and  $v_j$  is the input voltage to the  $j$ th motor. In these notations,  $j$  can be "2" or "s" referring to the motors providing the input torque to link 2 or the slider respectively. The full expressions of  $A$ ,  $B$ ,  $\frac{dA}{dt}$ , and  $\frac{dB}{dt}$  are

provided in the APPENDIX.

## IV. CONTROL STRATEGY

Although there are many other more accurate and advanced controllers that can be employed, PID controller is chosen because it is easy to be implemented and computationally efficient. In this case the control input to the motors is the voltage signal, which is governed by

$$u_{PIDj}(t) = k_{pj} e_j(t) + k_{dj} \dot{e}_j(t) + k_{ij} \int_0^t e_j(\tau) d\tau, \quad j = 2, s \quad (7)$$

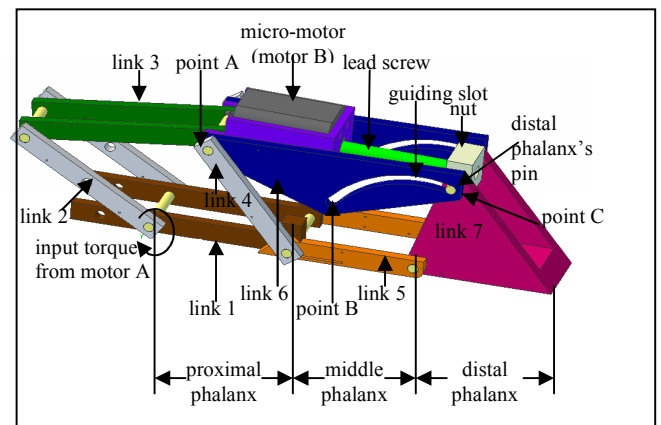


Fig. 1 Finger mechanism (add label no link)

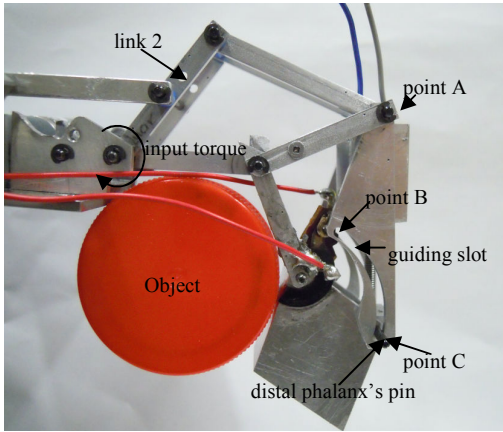


Fig. 2 Robotic finger during final grasping configuration

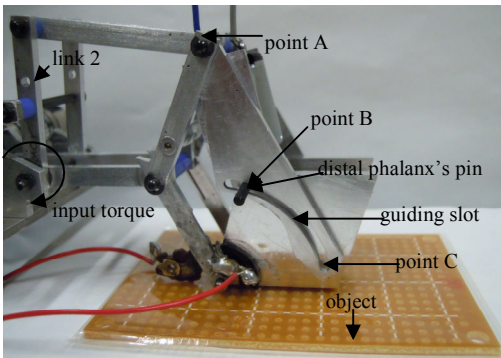


Fig. 3 Robotic finger during final pinching configuration

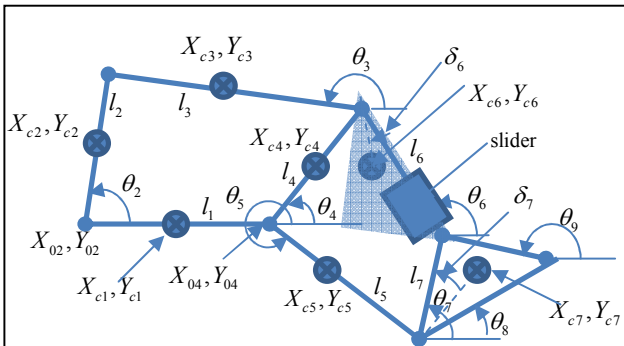


Fig. 4 Linkage parameters in mathematical modeling

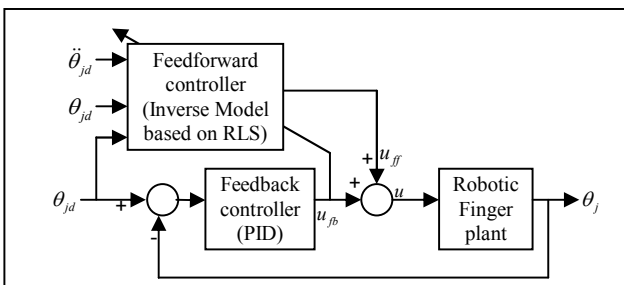


Fig. 5 RLS based FEL control scheme

where  $k_{pj}$ ,  $k_{dj}$  and  $k_{ij}$  are the positive proportional, derivative and integral gains of the PID controller respectively. The term  $e_j(t)$

is the difference between the reference,  $\theta_{jd}(t)$  and actual angular displacement,  $\theta_j(t)$  and  $\dot{e}_j(t)$  is its time derivative.

The RLS based FEL controller is implemented to overcome any parameter uncertainties present in the plant. It is a two degree of freedom control strategy which consists of feedforward and feedback control loops as illustrated in Fig. 5. The total control effort applied to the plant,  $u$  is the summation of the feedback and feedforward control outputs.

$$u = u_{ff} + u_{fb} \tag{8}$$

The PID feedback control loop can be implemented using any conventional controller. In this study, PID control algorithm governed by (7) is used to provide the feedback loop input signal,  $u_{fb}$ . The feedback loop ensures the stability of the whole system and acts as the learning signal for the feedforward loop. The RLS based feedforward controller learns the inverse model of the plant by trying to minimize the feedback control signal. If the inverse dynamic model is learned successfully, the ideal control input to produce the desired trajectory can be obtained by feeding the desired output to the feedforward loop controller. The feedforward control signal,  $u_{ff}$  can be represented as,

$$u_{ff}(t+1) = W^T(t+1)\Theta(t+1) \tag{9}$$

where  $W$  is the inverse plant parameter to be estimated and  $\Theta$  is the vector of the desired angular displacement, velocity and acceleration, described by

$$W = [w_1 \quad w_2 \quad w_3] \tag{10}$$

$$\Theta = [\theta_{jd} \quad \dot{\theta}_{jd} \quad \ddot{\theta}_{jd}]^T, \quad j = 2 \text{ or } s \tag{11}$$

During the learning process, the output of feedback loop is gradually minimized, while the output from the feedforward loop becomes the main control effort [10]. (RLS) algorithm is chosen for the learning process because it is simple to implement, provides fast convergence and does not require extensive learning parameter initialization.

The weight,  $W$  can be described mathematically in the recursive form as

$$W(t+1) = W(t) + P(t+1)\Theta(t+1)u_{fb}(t+1) \tag{12}$$

where the covariance matrix,

$$P(t+1) = \frac{1}{\lambda} \left[ P(t) - \frac{P(t)\Theta(t+1)\Theta^T(t+1)P(t)}{\lambda + \Theta^T(t+1)P(t)\Theta(t+1)} \right] \tag{13}$$

and  $\lambda$  is the forgetting factor chosen between 0 to 1. The value of  $\lambda < 1$ , allows training data from the early stages of learning, where the feedback error is large and most likely inaccurate to be neglected, by making the older values in the matrix  $P$  to be exponentially forgotten. If  $\lambda$  is set to 1, no forgetting takes place in the calculation process.

### V. EXPERIMENTAL SET UP

The experimental set up for the robotic finger control system is illustrated as in Fig. 6. It consists of the Matlab xPC Target system, power amplifier and the finger mechanism.

The Matlab xPC Target system is chosen to execute the control command to drive the robotic finger mechanism since it is easy to be implemented. It consists of a host PC and a target PC, installed with a National Instruments PCI-6251 data acquisition (DAQ) board. The host PC is installed with Matlab software and Simulink, Real-Time Workshop and xPC Target toolboxes. It provides the software environment to create the Simulink block diagram representing the control algorithm, compiles the programming algorithm into an executable code and uploads it to the target PC for real-time execution. The target PC specifically runs the controller program only. It reads the signals from the encoder and potentiometer, and provides the output control signals to the motors based on the pre-programmed control law in the host PC, through the DAQ board.

Since the output current from the DAQ board is limited to 0.005 A only, it is not enough to drive the motors. Therefore, the LM675 power amplifier is used to amplify the power in operating the motors. A dual power supply is used to provide power to the amplifier. The finger structure is made of aluminum, and small size with light weight actuators and sensors are chosen to achieve a compact finger design. The IG-13VM-SRP2004A-06 geared motor from Citizen Micro Co. Ltd, with a rated torque of 0.275 Nm is used as motor A. The geared motor is equipped with a 256 resolution encoder to measure the angular position of the motor. The slider

mechanism consists of a nut, a lead screw and an FF-030PK micro-motor with a torque of 0.00053 Nm at nominal speed manufactured by Mabuchi Motor Co. Ltd. The nut is custom made as shown in Fig. 7 so that it moves the distal phalanx along as it travels. The displacement of the slider and distal phalanx is measured from the resistance value of the rotary potentiometer attached to the distal phalanx. A pointer built on Link 5 and a voltage divider circuit are used to read the potentiometer resistance.

### VI. EXPERIMENTAL RESULTS

The finger is desired to track the reference trajectory given by

$$\theta_{2d} = \begin{cases} 0 & 0.6s \leq t \leq 2.1s \\ \frac{\pi}{4} \cos\left(\frac{2\pi}{3}t\right) - \frac{\pi}{4} + \theta_{2(0)} & 0.6s \leq t \leq 2.1s \end{cases} \quad (14)$$

$$l_{6d} = \begin{cases} -53.25t + 46.7 & 0s \leq t \leq 0.4s \\ 25.4 & 0.4s \leq t \leq 2.1s \end{cases}$$

The desired trajectory for the slider,  $\theta_{sd}$  is expressed in terms of  $l_{6d}$  using the relationship

$$l_{6d} = l_{6(0)} - P\theta_{sd} / (2\pi) \quad (15)$$

where  $l_{6(0)}$  is the length of link 6 at rest position and  $P$  is the lead screw pitch. The sampling time for the experiment has been set to 0.001s.

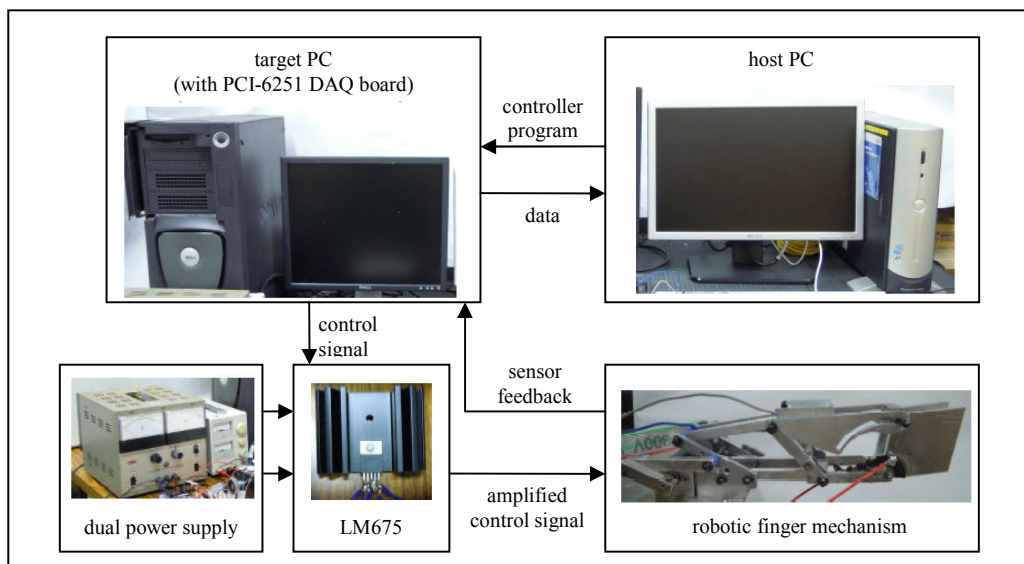


Fig. 6 Hardware set up

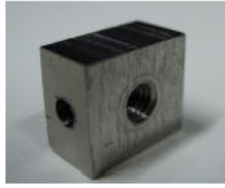


Fig. 7 Nut

The motor and linkage parameters are summarized in tables II and III respectively. The PID gains in controlling the angular displacement of link 2,  $\theta_2$  have been tuned manually as  $k_{p2}=100$ ,  $k_{i2}=10$  and  $k_{d2}=0.001$ . The same PID gains have been used in the FEL controller and the RLS parameters have been initialized as

$$P = \begin{bmatrix} 100 & 0 & 0 \\ 0 & 100 & 0 \\ 0 & 0 & 100 \end{bmatrix}, \quad W = \begin{bmatrix} 0 \\ 0 \\ 0 \end{bmatrix}, \quad \lambda = 1 \quad (16)$$

Fig. 8 illustrates experimental results of the angular displacement of link 2,  $\theta_2$  in tracking the reference trajectory. Although PID provides a satisfactory result, FEL controller gives a more accurate output since it overcomes the uncertainties present in the plant. The FEL control input in Fig. 9 shows that the feedforward loop has successfully learned the plant inverse dynamic as the feedback signal,  $u_{fb}$  approaches zero as the time increases and  $u_{ff}$  gradually becomes the main control effort.

The slider movement is controlled using PI controller by setting  $k_{ds}$  in (7) to 0 since the derivative term amplifies the noise effect present in potentiometer reading. The values of  $k_{ps}$  and  $k_{is}$  have been tuned manually to 6.15 and 0.0015 respectively. The control results and the voltage input are illustrated in figures 10 and 11 respectively. Since the result under PI controller had demonstrated a satisfactory tracking, the FEL controller was not implemented for controlling the slider position.

In this study, RLS algorithm has been chosen because it is easy to implement, provides fast convergence and does not require tedious learning parameter initialization. However, RLS is only efficient if the input or desired trajectory to the feedforward loop is persistently excited. For a non-persistently excited input, an advance controller is suggested for controlling  $\theta_2$  if a high tracking accuracy is desired.

TABLE III  
LINKAGE AND NUT PARAMETERS

$l_1$ : 27.3 mm,	$m_1$ : 2.1 g,	$j_1$ : $4.1 \times 10^2$ gmm <sup>2</sup> ,	$r_1$ : 19.4 mm,	$\delta_6$ : 0.02 rad
$l_2$ : 30.0 mm,	$m_2$ : 1.3 g,	$j_2$ : $1.3 \times 10^2$ gmm <sup>2</sup> ,	$r_2$ : 14.9 mm,	$\delta_7$ : 0.73 rad
$l_3$ : 36.2 mm,	$m_3$ : 1.6 g,	$j_3$ : $2.0 \times 10^2$ gmm <sup>2</sup> ,	$r_3$ : 17.9 mm,	
$l_4$ : 27.0 mm,	$m_4$ : 1.6 g,	$j_4$ : $9.9 \times 10$ gmm <sup>2</sup> ,	$r_4$ : 12.6 mm,	
$l_5$ : 24.0 mm,	$m_5$ : 1.1 g,	$j_5$ : $5.4 \times 10$ gmm <sup>2</sup> ,	$r_5$ : 10.2 mm,	
$l_{6(0)}$ : 46.7 mm,	$m_6$ : 18.2 g,	$j_6$ : $2.0 \times 10^3$ gmm <sup>2</sup> ,	$r_6$ : 15.4 mm,	
$l_7$ : 20.9 mm,	$m_7$ : 10.0 g,	$j_7$ : $1.2 \times 10^3$ gmm <sup>2</sup> ,	$r_7$ : 16.5 mm,	
$P$ : 0.5 mm	$m_c$ : 2.4 g,	$j_c$ : 1.5 gmm <sup>2</sup> ,		

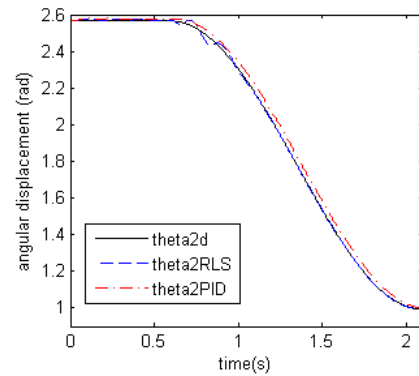


Fig. 8 Angular displacement of link 2,  $\theta_2$  under PID and FEL control

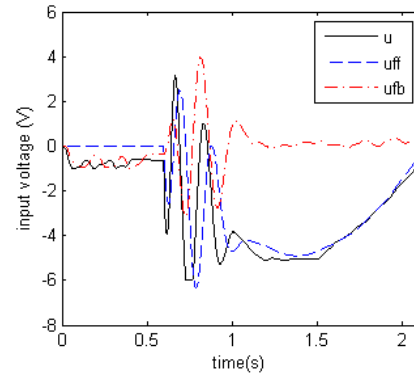


Fig. 9 Control input signal from FEL controller to motor A

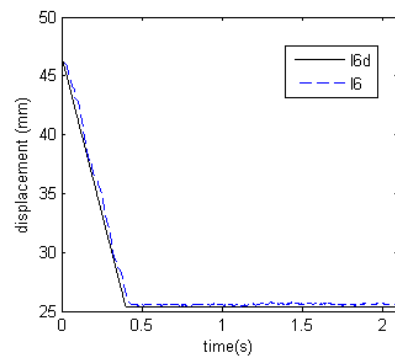
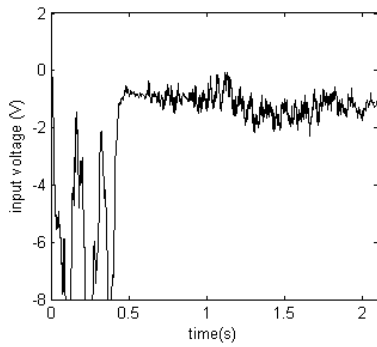


Fig. 10 Slider displacement,  $l_6$  under PID control


 Fig. 11 Input voltage to motor B,  $u_{PIDs}$ .

## VII. CONCLUSION

The experimental study of the position control of a compact robotic finger with self adaptive grasping and fingertip pinching during non-contact motion is presented in this paper. The position tracking for the angular displacement of link 2 under PID algorithm is satisfactory, but the RLS based FEL controller provides a more accurate results since it overcomes the uncertainties present in the plant. Although RLS algorithm is simple, provides fast convergence and does not require extensive learning parameter adjustment, it is limited for persistently excited reference trajectory only. In the cases where high accuracy tracking of non-persistently excited path is required, a more advance controller is suggested to serve this purpose. The experiment result shows that PI control scheme is efficient in controlling the slider movement. Future work involves the investigation of the finger force control algorithm while it is in contact with objects.

## APPENDIX

$$\begin{aligned}
 A = & C_1 + C_2 \left( \frac{\partial \theta_3}{\partial \theta_2} \right)^2 + (C_3 + C_5) \left( \frac{\partial \theta_4}{\partial \theta_2} \right)^2 \\
 & + C_4 \left( \frac{\partial \theta_3}{\partial \theta_2} \right) \cos(\theta_3 - \theta_2) + \left( \frac{\partial \theta_4}{\partial \theta_2} \right)^2 \left[ C_6 \left( \frac{\partial \theta_6}{\partial \theta_4} \right)^2 + C_7 \left( \frac{\partial \theta_7}{\partial \theta_4} \right)^2 \right. \\
 & \left. + C_8 \left( \frac{\partial \theta_6}{\partial \theta_4} \right) \cos(\theta_6 + \delta_6 - \theta_4) + C_9 \left( \frac{\partial \theta_7}{\partial \theta_4} \right) \cos(\theta_7 + \delta_7 - \theta_5) \right] \quad (17)
 \end{aligned}$$

where

$$\begin{aligned}
 C_1 = & m_2 r_2^2 + J_2 + m_3 l_2^2, \quad C_2 = m_3 r_3^2 + J_3, \quad C_3 = m_4 r_4^2 + J_4 \\
 C_4 = & 2m_3 l_2 r_3, \quad C_5 = m_5 r_5^2 + J_5 + m_6 l_4^2 + m_7 l_5^2, \quad C_6 = m_6 r_6^2 + J_6 \\
 C_7 = & m_7 r_7^2 + J_7, \quad C_8 = 2m_6 l_4 r_6, \quad C_9 = 2m_7 l_5 r_7 \quad (18)
 \end{aligned}$$

$$B = E_1 \left( \frac{\partial \theta_6}{\partial \theta_s} \right)^2 + E_2 \left( \frac{\partial \theta_7}{\partial \theta_s} \right)^2 \quad (19)$$

where

$$E_1 = m_6 r_6^2 + J_6, \quad E_2 = m_7 r_7^2 + J_7 \quad (20)$$

$$\begin{aligned}
 \frac{dA}{d\theta_2} = & 2C_2 \left( \frac{\partial \theta_3}{\partial \theta_2} \right) \left( \frac{\partial^2 \theta_3}{\partial \theta_2^2} \right) + 2(C_3 + C_5) \left( \frac{\partial \theta_4}{\partial \theta_2} \right) \left( \frac{\partial^2 \theta_4}{\partial \theta_2^2} \right) \\
 & + C_4 \left[ \frac{\partial^2 \theta_3}{\partial \theta_2^2} \cos(\theta_3 + \delta_3 - \theta_2) - \frac{\partial \theta_3}{\partial \theta_2} \sin(\theta_3 + \delta_3 - \theta_2) \left( \frac{\partial \theta_3}{\partial \theta_2} - 1 \right) \right] \\
 & + 2 \left( \frac{\partial \theta_4}{\partial \theta_2} \right) \left( \frac{\partial^2 \theta_4}{\partial \theta_2^2} \right) \left[ C_6 \left( \frac{\partial \theta_6}{\partial \theta_4} \right)^2 + C_7 \left( \frac{\partial \theta_7}{\partial \theta_4} \right)^2 \right. \\
 & \left. + C_8 \frac{\partial \theta_6}{\partial \theta_4} \cos(\theta_6 + \delta_6 - \theta_4) + C_9 \frac{\partial \theta_7}{\partial \theta_4} \cos(\theta_7 + \delta_7 - \theta_5) \right] \\
 & + \left( \frac{\partial \theta_4}{\partial \theta_2} \right)^2 \left\{ 2C_6 \left( \frac{\partial \theta_6}{\partial \theta_4} \right) \left( \frac{\partial^2 \theta_6}{\partial \theta_4^2} \right) + 2C_7 \left( \frac{\partial \theta_7}{\partial \theta_4} \right) \left( \frac{\partial^2 \theta_7}{\partial \theta_4^2} \right) \right. \\
 & \left. + C_8 \left[ \frac{\partial^2 \theta_6}{\partial \theta_4^2} \cos(\theta_6 + \delta_6 - \theta_4) - \frac{\partial \theta_6}{\partial \theta_4} \sin(\theta_6 + \delta_6 - \theta_4) \left( \frac{\partial \theta_6}{\partial \theta_4} - 1 \right) \right] \right. \\
 & \left. + C_9 \left[ \frac{\partial^2 \theta_7}{\partial \theta_4^2} \cos(\theta_7 + \delta_7 - \theta_5) - \frac{\partial \theta_7}{\partial \theta_4} \sin(\theta_7 + \delta_7 - \theta_5) \left( \frac{\partial \theta_7}{\partial \theta_4} - 1 \right) \right] \right\} \quad (21)
 \end{aligned}$$

$$\frac{dB}{d\theta_s} = 2E_1 \frac{\partial \theta_6}{\partial \theta_s} \frac{\partial^2 \theta_6}{\partial \theta_s^2} + 2E_2 \frac{\partial \theta_7}{\partial \theta_s} \frac{\partial^2 \theta_7}{\partial \theta_s^2} \quad (22)$$

## REFERENCES

- [1] K. Hoshino, I. Kawabuchi, "Dexterous Robot Hand with Pinching Function at Fingertips", in 2006 *IEEE/RAS-EMBS International Conference on Biomedical Robotics and Biomechatronics*, pp. 1113-1118.
- [2] S. G. Jacobsen, E. K. Iversen, D. F. Knutti, R. T. Johnson, K. B. Biggers, "Design of the Utah/M.I.T. Dextrous Hand", in 1986 *IEEE International Conference on Robotics and Automation*, pp.1520-1532.
- [3] M. T. Mason, J. K. Salisbury, *Robot Hands and the Mechanics of Manipulation*. USA: MIT Press, 1985.
- [4] B. Massa, S. Rocella, M. C. Carozza and P. Dario, "Design and Development of an Underactuated Prosthetic Hand", in 2002 *IEEE International Conference on Robotics and Automation*, pp. 3374-3379.
- [5] N. Fukaya, S. Toyama, T. Asfour and R. Dillmann, "Design of the TUAT/ Karlsruhe Humanoid Hand", in the *Proceedings of the 2000 IEEE/RSJ International Conference on Intelligent Robots and Systems*, 2000, pp. 1754- 1759.
- [6] N. Z. Azlan and H. Yamaura, "Modeling and Control of Compact Anthropomorphic Robot Finger", *Proceedings of the 2000 International Conference of Modelling, Identification and Control*, 2011, pp 118-123.
- [7] J. Tao and J. P. Sadler, "Constant Speed Control of a Motor Driven Mechanism System", *Mechanism and Machine Theory*, vol 30, pp737-748, 1994.
- [8] M. C. Lin and J. S. Chen, "Experiments toward MRAC design for linkage system", *Mechatronics*, vol. 6, no. 8, pp933-953, 1996.
- [9] L. C. Dugler, A. Kirecci and M. Topalbekiroglu, "Modeling and simulation of hybrid actuator", *Mechanism and machine theory*, vol. 38, pp 395-407, 2003.
- [10] H. Chen, K. Hirasawa and J. Hu, "Robust Feedback Error Learning Method for Controller Design of Nonlinear Systems", 2004 *IEEE International Joint Conference on Neural Networks*, 2004, pp1835-40.